

Light-Metal Functionalized Boron Monoxide Monolayers as Efficient Hydrogen Storage Material: Insights from DFT Simulations

Wael Othman^{1,2}, Wadha Al Falasi^{3,4}, Tanveer Hussain⁵, and Nacir Tit^{3,4*}

¹ Engineering Division, New York University Abu Dhabi, Abu Dhabi, United Arab Emirates

² Mechanical and Aerospace Engineering, Tandon School of Engineering, New York University,
NY 10012, USA

³ Physics Department, UAE University, Al Ain, United Arab Emirates

⁴ Water Research Center, UAE University, Al-Ain, United Arab Emirates

⁵ School of Science and Technology, University of New England, Armidale, New South Wales,
2351, Australia

*Corresponding Author: ntit@uaeu.ac.ae

Abstract

Exceptionally high energy density by mass, natural abundance, widespread applications, and environmental friendliness make hydrogen (H₂) a front-runner among clean energy options. However, the transition toward clean and renewable energy applications and the actualization of H₂ economy require an efficient H₂ storage medium. Material-based H₂ storage is a viable option, as liquefaction and storage under pressure require ultra-low temperature (-253 °C) and tremendously high pressure (700 atm), respectively. In this work, we highlight the exceptional H₂ storage capabilities of recently synthesized boron monoxide (BO) monolayer functionalized with light metals (Li, Na, K, and Ca). Our computational approach, employing density functional theory (DFT), *ab initio* molecular dynamics (AIMD), and thermodynamic analysis, reveals promising results. We found that up to four metal dopants (Li, Na, K, and Ca) can be adsorbed onto BO monolayer with significantly strong binding energies (-2.02, -1.53, -1.52, and -2.24 eV per dopant, respectively). Importantly, these bindings surpass the cohesive counterparts of the parental metal bulks, consequently stabilizing the crystal integrities, as confirmed by AIMD simulations. Each metal dopant on BO efficiently adsorbs multiple H₂ molecules through electrostatic and van der Waals interactions. Interestingly, the metal-functionalized BO monolayers exhibit exceptionally high H₂ gravimetric capacities of 11.75, 9.52, 9.80, and 11.43 wt% for 4Li, 4Na, 4K, and 4Ca@BO, respectively. These promising capacities exceed the 5.50 wt% target set by the US Department of Energy for 2025. Following the same guidelines, the average binding energy per H₂ molecule is within the range of -0.17 to

-0.32 eV. The adsorption and desorption of H₂ under practical working conditions are investigated by Langmuir adsorption model based statistical thermodynamic analysis, further supporting the potential of metal-functionalized BO monolayers for material-based H₂ storage applications.

PAC Numbers: 31.15.E; 68.43.-h; 68.43.Mn; 68.65.Pq; 73.43.Cd; 75.70.Rf

Keywords: Density functional theory, Hydrogen storage, 2D materials, Metal Functionalization, Boron Monoxide, *Ab initio* molecular dynamics, Thermodynamics

I. Introduction

The substantial increase in global energy demand has led to a 1.0 °C rise in global temperature and a simultaneous increase in sea levels, primarily attributed to excessive fossil fuel usage and its associated greenhouse gas emissions [1]. In an effort to address global warming and climate change challenges, renewable and clean energy resources like solar, wind, and hydropower are substituting fossil fuels. These sustainable alternatives offer the dual benefits of fulfilling future energy demands and preserving the environment [2]. However, the intermittent nature of sustainable energy sources underscores the crucial need for energy storage solutions with high efficiency, sustainability, and eco-friendliness. In contrast to traditional energy storage, hydrogen (H₂) has emerged as the most promising candidate thanks to its ultra-high energy density by mass, abundance, and environmental friendliness [3]. The production of H₂ through water electrolysis only emits oxygen (O₂), and its combustion in fuel cells produces solely water (H₂O), making it a carbon-free energy carrier [4-6]. As fuel cell vehicles (FCVs), including cars, buses, trains, and airplanes, have entered the race towards sustainable transportation, their effective implementation relies heavily on practical H₂ storage, a key focus in current research themes [7].

The challenge of H₂ storage arises from its low density in gaseous form at ambient pressure and temperature, approximately 1/14th compared to air density [8]. Conventional H₂ storage methods typically involve pressurized tanks or liquification. However, these technologies raise safety concerns and struggle to store hydrogen cost-effectively for extended periods. For instance, storing hydrogen as a gas typically requires gigantic tanks with high pressures ranging from 350 to 700 bar to hold a practical amount of H₂ [8]. Meanwhile, FCVs currently rely on pressurized H₂ in vessels, requiring an average of 9 kg of H₂ for a 500 km driving range [8]. The intrinsic limitations of pressurized tank storage result in insufficient volumetric and gravimetric storage densities, along with safety considerations. On the other hand, storing hydrogen as a liquid requires cooling it down to cryogenic temperatures (-252.8 °C).

Concerns regarding safety and overall cost in conventional H₂ storage have urged the exploration of alternative storage technologies [9-10]. In this context, material-based (solid-state) H₂ storage becomes the most viable option to minimize the volume and power required for practical H₂ storage conditions. Ideally, storage materials should achieve high storage capacity, rapid chemical kinetics, and a reversible low dehydrogenation temperature. These characteristics depend on the number of chemically reactive sites and binding between the host material and H₂ molecules. In this regard, materials with a high surface area are advantageous in maximizing the number of stored H₂ molecules. At the same time, the type of binding (physisorption or chemisorption) influences the chemical kinetics and adsorption-desorption reversibility. According to the Langmuir equation, moderate binding energies of H₂ molecules on the storage medium should be around 0.155 eV/atom, or 14.96 kJ/mol, to achieve appropriate reversibility under practical conditions around 30 bar and 298 K [11]. Additionally, a moderate interaction between the host material and H₂ molecules is required to ensure strong physisorption, with adsorption energy in the 0.15–0.60 eV/H₂ range, along with sufficient gravimetric density to surpass the United States Department of Energy (US-DoE) goal of 5.5 wt% [12, 13].

Various materials, including metal hydrides and porous nanomaterials, have been proposed as promising mediums for H₂ storage, where hydrogen is stored either on the surfaces (adsorption) or within solids (absorption). However, inherent limitations, such as low storage capacity, slow chemical kinetics, and elevated reversible dehydrogenation temperatures, hinder their practical applications [13]. Among the available options, two-dimensional (2D) materials stand out due to their lower mass density and ultra-high surface areas reaching 2078 m²/g for boron nitride (BN) [14] and 2630 m²/g for graphene [15]. While the pristine forms of the most 2D materials weakly interact with H₂ molecules [16-19], doping with alkali, alkaline-earth, or transition metals serves as a promising approach to intensify H₂ bindings [20-23]. The low electronegativities of such metals induce strong polarization, enhancing the attraction of H₂ molecules (electrostatic and van der Waals interactions) and overall H₂ storage performance, as demonstrated with functionalized B₂O [24], graphene [25], haeckelite [26], Ene–Yne [27], C₂N [28, 29], BN [30], and phosphorene [31].

Recent literature reports significant progress in utilizing 2D materials for H₂ storage. For instance, polar 2D materials, particularly functionalized MXenes and transition metal dichalcogenides (TMDs), appear to be highly promising [10, 32-34]. Kumar and co-workers [10] have shown that Ti₂C MXene can achieve an uptake capacity of up to 8.6 wt%, which is higher than the gravimetric capacity of metal-based complex hybrids (~5.5 wt%). Zhu *et al.* [35] demonstrated the high potential of TMDs as cost-effective catalysts for

the hydrogen evolution reaction (HER), showcasing stable adsorption of a substantial number of H₂ molecules on 1T-MoS₂ with appropriate adsorption energy. In a separate study, Wang *et al.* [36] discovered that MoS₂ nanotubes (NT) effectively attract H₂ and methane molecules to both outer and inner surfaces, reporting hydrogen storage capacity in the range of 0.7-0.9 wt% depending on the nanotube diameter. Recently, Alfalasi *et al.* showed that doping the Se sites in the combined MoSe₂/Graphene bilayer with Mn improves the gravimetric H₂ capacity, primarily attributed to enhanced electric dipole moments in the TMD monolayer [32]. These studies underscore the growing interest in utilizing 2D materials for H₂ storage applications, highlighting their potential to propel advancements in energy storage technologies.

Nevertheless, 2D materials consisting of heavy elements exhibit limited H₂ storage capacities, such as GeC [37], SnC [38], and MoS₂ [39]. On the other hand, certain carbon-based nanostructures, such as carbon nanotubes [40], fullerene [40, 41], and graphene [42]. show weak interactions towards H₂ molecules, and result in low storage capacities. Heavy transition metals usually possess high cohesive energies and favor clustering instead of homogeneously distributing over the storage materials, resulting in sluggish reversibility and low storage capacity [43]. Considering these factors, 2D materials composed of light atoms and functionalized with light alkali or alkaline-earth metals emerge as ideally feasible candidates for achieving high H₂ storage capacities.

In 2023, Perras *et al.* [44] employed advanced multidimensional nuclear magnetic resonance methods to unravel the atomic structure of boron monoxide (BO), a material initially reported in 1940 [45] and synthesized in 1955 [46]. The recent material characterization revealed the presence of interconnected B₄O₂ rings forming two-dimensional nanosheets of BO [44]. The large pores within BO act as attraction sites for alkali and alkaline-earth metals. This makes the material highly promising for H₂ storage, representing a potential application that had not been previously explored. Motivated by these intriguing properties, this study showcases the significant potential of recently synthesized BO monolayers in H₂ storage applications using the Vienna Ab initio Simulation Package (VASP). Our theoretical analysis utilizes state-of-the-art tools, including density-functional theory (DFT), *ab initio* molecular dynamics (AIMD), and thermodynamic analysis, to assess effective hydrogenation uptake capacity. By embedding multiple light metal atoms (Li, Na, K, and Ca) into the large pores of BO sheets, our findings indicate that the ionic bindings exceed the cohesive energies of the corresponding bulk metals. This prevents metal clustering and stabilizes the crystal integrity of metal-functionalized BO, making it well-suited for H₂ storage with high gravimetric uptake capacities of up to 11.75 wt%. As a result, metal-functionalized BO emerges as a

promising class of non-precious 2D materials for hydrogen storage functionality, filling the gap in materials-based clean energy storage.

II. Computational Methods

To unravel the H₂ storage capabilities of BO, we conducted spin-polarized DFT calculations involving atomic structure optimization, adsorption mechanism, charge transfer analysis, and electronic properties assessments. These calculations were performed using the VASP within the frameworks of DFT and the projected augmented plane wave (PAW) method [47]. The Perdew-Burke-Ernzerhof form of the generalized gradient approximation (PBE-GGA) approach was used to address the exchange-correlation energy [48]. Given that weakly-dispersive van der Waals interactions play a crucial role in the intrinsic attractive forces, we incorporated the DFT-D3 method of Grimme to obtain reliable adsorption energies [49]. The modeled structures throughout this study were based on the relaxed unit cell of BO, having square 2D-Bravais lattice structure with lattice parameter $a = b = 7.826 \text{ \AA}$ and a basis of eight B and eight O atoms. Adequate 15- \AA vacuum space was added to the vertical direction of the BO to eliminate the self-interactions among the periodically adjacent layers. For the structural relaxation, we applied the convergence tolerances for the total energy of 10^{-6} eV and atomic force of 0.01 eV/ \AA . In sampling the Brillouin zone, we utilized the Monkhorst-Pack technique with $5 \times 5 \times 1$ K-grid during geometry optimization [50]. A denser K-point grid of $8 \times 8 \times 1$ was used for the density of states (DOS) calculations. The cut-off energy of the plane-wave was 500 eV. Bader-charge analysis within the framework of VASP was applied to calculate the charge exchange between H₂ molecules and the host medium [51].

The average binding energy (E_{bind}) of a metal atom (M) embedded in the pores of BO monolayer substrate were calculated using the formula:

$$E_{bind} = \frac{E_{BO+nM} - (E_{BO} + nE_M)}{n} \quad (1),$$

where E_{BO+nM} , E_{BO} , E_M stand for the total energies of the system of BO embedded with n metal atom(s), pristine BO, and isolated metal atom, respectively. Moreover, *ab initio* molecular dynamics (AIMD) was performed to further validate the structural stabilities of metal-functionalized BO at 400 K. Nose-Hoover thermostat was employed to control the temperature, with a time step of 1.0 fs and for 8 ps.

The average adsorption energy (E_{ads}) of H₂ molecule on top of the substrate is defined as:

$$E_{ads} = \frac{E_{Sheet+mH_2} - (E_{Sheet} + mE_{H_2})}{m} \quad (2),$$

where, $E_{Sheet+mH_2}$, E_{Sheet} , E_{H_2} are the total energies of the mH_2 molecule(s) adsorbed on the BO (adsorbent), the BO, and the isolated H_2 molecule, respectively. The uptake gravimetric capacity is defined as follows [32]:

$$C_T(\text{wt}\%) = \left[\frac{N_T \cdot M(H_2)}{N_T \cdot M(H_2) + N_{metal} \cdot M(\text{metal}) + N_{BO} \cdot M(\text{BO})} \right] \times 100\% \quad (3),$$

where $M(H_2)$, $M(\text{metal})$, and $M(\text{BO})$ stand for the molecular masses of H_2 molecule, metal adatom, and host crystal BO, whereas N_T , N_{metal} , and N_{BO} stand for the number of H_2 molecules, metal adatoms, and BO pairs in the substrate.

The adsorption-desorption characteristics at operational conditions were analyzed by statistical thermodynamics according to the grand canonical partition function (z):

$$z = 1 + \sum_{i=1}^n e^{-\frac{(E_b^i - \mu)}{k_B T}} \quad (4),$$

where n represents the maximum number of adsorbed H_2 molecules, whereas E_b^i , k_B , μ , and T represent the adsorption energy of the i^{th} adsorbed H_2 molecule, the Boltzmann constant (1.38×10^{-23} J/K), chemical potential of the gas phase of the H_2 molecule, and absolute temperature, respectively. In particular, μ is a function of P and T , defined as:

$$\mu_{H_2}(P, T) = \Delta H + T\Delta S + k_B T \ln \frac{P}{P_0} \quad (5),$$

where ΔH , ΔS , P , and P_0 represent the enthalpy change, entropy change, pressure, and the atmospheric pressure (1.01×10^5 Pa), respectively. The values of $\Delta H + T\Delta S$ are obtained from the experimental database [43]. Meanwhile, the number of stored H_2 molecules (N) in the host material can be expressed by:

$$N = N_0 \left[\frac{z-1}{z} \right] \quad (6),$$

where N_0 represents the maximum number of H_2 molecules adsorbed on the host medium at 0 K (N_T).

III. Results and Discussion

(a) Pristine BO Monolayer Properties

Pristine boron monoxide (BO) monolayer crystallizes in a square Bravais lattice with a basis comprising eight B and eight O atoms. This structure belongs to the space group P4/mmm (No. 123) [52]. **Figure 1(a)** shows the relaxed atomic structures using PBE-DFT method. The bond length B-O within 1.37-1.39 Å and the lattice constant of $a = 7.83$ Å are consistent with both original synthesized structure [44] and *ab initio* predictions [52]. **Figures 1(b)** and **1(c)** show the corresponding spin-polarized band structure and projected density of states (PDOS), respectively. The band structure shows that BO is wide-bandgap semiconductor with an indirect bandgap of energy $E_g = 2.23$ eV (i.e., the valence-band maximum (VBM) is at Γ point and the conduction band minimum (CBM) is at M point of the Brillouin zone). This value of bandgap energy is underestimated as being calculated using PBE-DFT method. Yet this value is consistent with the first-principles results of 2.18 eV reported by Mortazavi et al. [52]. These latter authors further involved HSE06 hybrid functional to improve the bandgap and reported $E_g = 3.78$ eV, in agreement with the experimental value. Furthermore, the spin-polarized PDOS, shown in **Figure 1(c)**, confirms that BO is a paramagnetic wide-bandgap semiconductor. The near VBM states have equal contributions from p_x and p_y orbitals of both B and O atoms, whereas the near CBM states receive contributions from p_z states of boron more than oxygen atoms. Hence, the PDOS reveal that BO is a covalent material with partial ionic character, as oxygen possesses more electronegativity than boron (i.e., $\chi^B = 2.04$ Pauling and $\chi^O = 3.44$ Pauling [53]).

It is customary, first, to assess the adsorption of a single H₂ molecule on pristine material. Hence, on the primitive cell shown in dashed line in Figure 1a, we carried out the relaxation of a single H₂ molecule on various possible sites, as indicated in **Figure S1(a)** (supporting information). All the adsorption processes led to physisorption types, with adsorption energies shown in chart diagram of **Figure S1(b)** (supporting information). It seems that two adsorption sites are favorable and do correspond to the centres of the two biggest pores (X6, and X7), having adsorption energies of values $E_{ads} = -0.158$ eV and -0.159 eV, respectively. We decided to set the threshold energy at -0.16 eV in our study of uptake capacity shown below. Of course, the threshold energy is arbitrary chosen in many research groups. Nonetheless, in our case, the value has significance; after the functionalization of BO, all absolute values of average adsorption energies larger than this threshold should be considered an improvement over the pristine case of adsorption. Meanwhile, these adsorption energies of a single H₂ molecule on pristine BO are below the energy range $[-0.6, -0.2]$ eV set by the US-DoE as recommended for hydrogen storage applications. So, one way to enhance the adsorption energy is to consider the functionalization of BO with alkali and rare earth alkaline metals (such as Li, Na, K, and Ca). We emphasize that this selection of metal is intended to exclude the transition metals in order to avoid the chemisorption processes. So, the selected light atoms

are expected to alter the bonding with the lattice and contribute to the formation of electric dipole moments to make the substrate even more polar. The enhancement in the polarity of the surface could induce dipole moments into the H₂ molecules, as will be indicated by the enhancement in the adsorption energy described below.

(b) Light Metal Functionalization

The primitive cell of BO possesses two hexagons (B₄O₂), one intermediate pore (B₈O₄) and one large pore (B₈O₈), as shown in **Figure 1(a)**. The light metal atoms (X = Li, Na, K, and Ca) can be embedded in the latter two pores and decorated on the former two hexagons. Hence, **Figure 2** and **Figure S2** (supporting information) show the optimized atomic structures of metal-functionalized BO. We have functionalized the BO primitive cell one by one of light metal atoms up to 4 atoms at maximum (referred as 4X@BO). As expected, the first two light metal atoms got fully embedded in the two large pores and stabilize within the same membrane as BO monolayer. Meanwhile, the next two light metal atoms were just decorated on the top of the two B₄O₂ hexagons (see **Figure S2** and **Figure 2**). The average E_{bind} of these metal adatoms were calculated using equation (1), and the absolute values were found to be stronger than the cohesive energy of the corresponding bulk metals (i.e., $|E_{bind}^{ave}| > |E_{coh}|$, for up to 4 light metal atoms), as shown in **Figure 3(a)**. In each case, a maximum of four light metal atoms of Li, Na, K, and Ca are found bonded with the BO, resulting in strong E_{bind} values of -2.02, -1.53, -1.52, and -2.24 eV per dopant, respectively. It is worth emphasizing that the average E_{bind} is more relevant than the recursive E_{bind} as it better simulates the experimental synthesis of functionalization more realistically. The fact that $|E_{bind}| > |E_{coh}|$ should reveal that the metal dopants are more inclined to bind to the lattice rather than clustering. This fosters the stability of light-metal functionalized BO sheets, thereby increasing their viability for hydrogen storage. While metal functionalization induces buckling in the atomic structures of BO sheets, our AIMD analysis, conducted at 400 K for 8 ps by a step of 1 fs, indicates insignificant fluctuations in the total energies during the simulation, as depicted in **Figure 3(b)**. This further confirms the structural integrity of metal-functionalized BO over time. It is noteworthy that Mg exhibited weak E_{bind} to the BO sheet, leading to its exclusion from the list of selection of catalyst candidates.

Moreover, the results of the spin-polarized band structure and PDOS calculations, shown in **Figure 4**, reveal significant alterations in the electronic properties of BO upon metal functionalization, which characterize the chemical bonds and support the strong E_{bind} . The absence of the band gap indicates the induced metallization of all 4X@BO systems. However, in the case of 4Na and 4K@BO, split bands (half-metallicity) persist for spin-down electrons, with energy values of 0.182 and 0.230 eV, respectively.

Meanwhile, the spin-polarization calculations provide information about the magnetization, which contributes to the interaction with H₂ molecules, particularly in the cases of 4K, 4Li, and 4Na@BO with total magnetization of 2.109, 1.062, 0.03 μ_B , respectively. **Table 1** summarizes the electronic properties (Bader charge transfer, band-gap energy, and total magnetization) of pristine BO and light-metal functionalized BO (i.e., 4X@BO, with X = Li, Na, K, and Ca).

Additionally, we conducted calculations of charge density difference (CDD) to understand the binding nature of metal atoms to the BO lattice. **Figure 5** presents the calculated CDD, showing the bond characteristics of maximally localized Wannier functions (MLWFs). In particular, the Wannier orbitals in Li- and Ca-decorated BO in **Figures 5(a)** and **5(d)** exhibit an enhanced population of the positive value (yellow) and gain of charge, whereas those in Na- and K-decorated BO in **Figures 5(b)** and **5(c)** show a more spherical shape of the negative value (cyan) and charge deficit.

(c) Hydrogenation of 4X@BO

The H₂ storage capacities of the 4X@BO are subsequently evaluated. In **Figure 6**, the optimized atomic structures showcase the maximum number of H₂ molecules adsorbed on the 4X@BO systems. Additionally, **Figure 7(a)** shows the absolute values of the corresponding average adsorption energies. It is worth mentioning here that H₂ adsorption is carried out in stepwise manner. Initially, a single H₂ molecule is introduced to each metal dopant, a total of 4H₂ on 4X@BO, and the systems are completely optimized. Next, the number of H₂ are increased to 2, 3, 4, and 5 per metal dopant on 4X@BO, and structural relaxations are performed in each situation. In each case, the E_{ads} values (per H₂) are calculated by equation (2) and compared with the threshold value of -0.160 eV/H₂. Our results suggest that Li-, Na-, K-, and Ca-decorated BO can adsorb up to 16, 16, 20, and 24 H₂ molecules, respectively. These H₂ molecules are physisorbed on the 4X@BO *via* the predominant electrostatic and van der Waals-type interactions. The average E_{ads} values are -0.205, -0.175, -0.185, and -0.204 eV for fully hydrogenated 4Li, 4Na, 4K, and 4Ca@BO, respectively, exceeding the -0.160 eV threshold in magnitude.

Subsequently, the maximum numbers of stored H₂ molecules (N_T) are used to calculate the theoretical H₂ gravimetric capacities (C_T) according to equation (3). All atomic weights are sourced from the database [54]. As shown in **Figure 7(b)**, the theoretical gravimetric capacities are 11.75, 9.52, 9.80, and 11.43 wt%, corresponding to 4Li, 4Na, 4K, and 4Ca@BO, respectively. It is important to acknowledge that DFT utilizes the Born-Oppenheimer frozen lattice approximation, wherein all calculations are performed at 0 K. These theoretical capacities exclude the essential thermodynamic contributions of finite pressure and temperature.

(d) Thermodynamic analysis

Since it is crucial to understand the effective H₂ storage capacity of the proposed materials at ambient conditions of practical temperature and pressure, we conducted a statistical thermodynamic analysis based on the Langmuir adsorption model [55-57]. **Figure 8** shows, based on equations (4-6), the number of H₂ molecules (N) adsorbed at given P and T values (*i.e.*, N-P-T diagram) on the BO primitive cell with 4 metal dopants (*i.e.*, 4X@BO, X = Li, Na, K, and Ca). Remarkably, the H₂ molecules can be released from the storage material under high-temperature and low-pressure conditions, or else they can be stored in low-temperature and high-pressure conditions. Furthermore, one can assess the realistic absorption-desorption characteristics of the adsorbed H₂ molecules. In practice, the pressure (P) and temperature (T) of adsorption are 30 atm and 25 °C, respectively whereas those of desorption are 3 atm and 100 °C, respectively [58]. Accordingly, **Table 2** compiles the calculated theoretical storage at 0 K (C_T) and effective storage (C_E) at the practical adsorption and desorption conditions. The obtained effective H₂ gravimetric capacities of 4Li, 4Na, 4K, and 4Ca@BO are 9.88, 3.96, 8.53, and 9.78 wt%, respectively. Notably, the capacities of BO sheets decorated with 4Li, 4K, and 4Ca surpass the goal value of 5.5 wt% set by the US-DoE for 2025 [24]. In **Table 3**, we present a comprehensive comparison between our results using DFT and those from similar DFT studies of different 2D materials reported in the literature. Overall, our theoretical gravimetric capacity of 4X@BO is almost always higher than in many DFT-studied materials. Besides, it is remarkable that in the few cases of materials whose gravimetric capacities are higher than ours, the authors carried out the hydrogenation to much lower threshold average adsorption energies. Thus, our 4X@BO systems can potentially surpass these systems by accommodating more H₂ molecules and lowering the average E_{ads} even further below our set threshold energy (-0.16 eV/ H₂ molecule). Based on our findings, it is thus conclusive that BO sheets functionalized with alkali and alkaline-earth metals are promising materials for hydrogen storage applications.

IV. Conclusions

In this study, we demonstrated the remarkable H₂ storage efficiency of BO monolayers functionalized with Li, Na, K, Ca. Utilizing a comprehensive set of theoretical approaches, including DFT, AIMD, and thermodynamic analysis, we investigated the theoretical and effective H₂ storage capacities of 4X@BO at ambient conditions. Our findings revealed that the presence of pores in BO monolayer induces robust ionic bonds with all the light metal dopants, while having average binding energies that surpass the cohesive energies of the corresponding bulk metals. This criterion simultaneously prevents the formation of metal clusters and guarantees the stable crystal integrity of 4X@BO. The thermal stabilities of 4X@BO were

confirmed through AIMD at 400K. The semiconducting to metallic transition of BO upon the metal functionalization was caused by the significant charge transfer from the dopants to the monolayer. We found that 4X@BO adsorbed a large number of H₂ with desirable average adsorption energies of -0.205, -0.175, -0.185, and -0.204 eV for fully hydrogenated 4Li, 4Na, 4K, and 4Ca@BO, respectively. It was observed that Li- and Ca-decorated BO monolayer exhibit theoretical H₂ storage capacities of 11.75 and 11.43 wt%, respectively, exceeding the US-DoE goal of 5.50 wt% by 2025. Consequently, 4X@BO emerges as a promising class of 2D materials for H₂ storage applications. The insights gained from our theoretical calculations will guide the synthesis of efficient materials for high reversible capacity in H₂ storage applications at practical operating conditions.

Acknowledgements

The authors are indebted to thank Dr. Thomas Fowler for critical reading of the manuscript and the National Water and Energy Center (NWECC) at the UAE University for the financial support (Grant number: 12R162).

Author Contributions:

Wael Othman: Investigation, Formal analysis, Methodology, Visualization, Validation, Project administration, Software, Writing - original draft preparation. **Wadha Al-Falasi:** Investigation, Formal analysis, Methodology, Validation. **Tanveer Hussain:** Conceptualization, Investigation, Formal analysis, Methodology, Resources, Writing- Reviewing and Editing. **Nacir Tit:** Conceptualization, Funding acquisition, Resources, Supervision, Writing- Reviewing and Editing.

Competing Interests:

The authors declare that they have no known competing financial interests or personal relationships that could have appeared to influence the work reported in this paper.

Supplementary Documents:

Figure S1: (a) Relaxed atomic structures (top and side views) and (b) the corresponding adsorption energy of one H₂ molecule on different sites of pristine BO.

Figure S2: Optimized atomic structures (top and side views) of BO decorated with 1, 2, and 3 ad-atoms of (a) Li, (b) Na, (c) K, and (d) Ca (primitive cell represented by the dashed box).

References

- [1] S. Fawzy, A.I. Osman, J. Doran, D.W. Rooney, Strategies for mitigation of climate change: a review, *Environ. Chem. Lett.* 18 (2020) 2069-2094.
- [2] A.D. Sakti, P. Rohayani, N.A. Izzah, N.A. Toya, P.O. Hadi, T. Octavianti, W. Harjupa, R.E. Caraka, Y. Kim, R. Avtar, N. Puttanapong, C.H. Lin, K. Wikantika, Spatial integration framework of solar, wind, and hydropower energy potential in southeast asia, *Sci. Rep.* 13 (2023) 340.
- [3] T. He, P. Pachfule, H. Wu, Q. Xu, P. Chen, Hydrogen carriers, *Nature Rev. Mater.* 1 (2016) 16059.
- [4] J.M. Ogden, Hydrogen: The fuel of the future? *Phys. Today.* 55 (2002) 69-75.
- [5] B. Johnston, M.C. Mayo, A. Khare, Hydrogen: the energy source for the 21st century, *Technovation* 25 (2005) 569-585.
- [6] M.K. Singla, P. Nijhawan, A.S. Oberoi, Hydrogen fuel and fuel cell technology for cleaner future: a review, *Environ. Sci. Pollut. Res.* 28 (2021) 15607-15626.
- [7] T. Kaewmaraya, N. Thatsami, P. Tangpakonsab, R. Kinkla, K. Kotmool, C. Menendez, K.-F. Aguey-Zinsou, T. Hussain, Ultrahigh hydrogen storage using metal-decorated defected biphenylene, *Appl. Surf. Sci.* 629 (2023) 157391.
- [8] Y.J. Huang, Y.H. Cheng, J.Y. Zhang, A review of high density solid hydrogen storage materials by pyrolysis for promising mobile applications, *Ind. Eng. Chem. Res.* 60 (2021) 2737-2771.
- [9] K. Ledwaba, S. Karimzadeh, T.-C. Jen, Emerging borophene two-dimensional nanomaterials for hydrogen storage, *Mater. Today Suitainability* 22 (2023) 100412.
- [10] P. Kumar, S. Singh, S.A.R. Hashmi, K.H. Kim, MXenes: Emerging 2D materials for hydrogen storage, *Nano Energy* 85 (2021) 105989.
- [11] S.K. Bhatia, A.L. Myers, Optimum Conditions for *Adsorptive* Storage, *Langmuir* 22 (2006) 1688-1700.
- [12] H. Si, L.J. Peng, J.R. Morris, B.C. Pan, Theoretical prediction of hydrogen storage on ZnO sheet, *J. Phys. Chem. C* 115 (2011) 9053-9058.
- [13] J. Chen, J. Cao, J. Zhou, Y. Zhang, M. Li, W. Wang, J. Liu, X. Liu, Mechanism of highly enhanced hydrogen storage by two-dimensional 1T' MoS₂. *Phys. Chem. Chem. Phys.* 22 (2020) 430-436.
- [14] J. Li, X. Xiao, X. Xu, J. Lin, Y. Huang, Y. Xue, P. Jin, J. Zou, C. Tang, Activated boron nitride as an effective adsorbent for metal ions and organic pollutants, *Sci. Rep.* 3 (2013) 3208.
- [15] M.D. Stoller, S. Park, Y. Zhu, J. An, R.S. Ruoff, Graphene-Based Ultracapacitors, *Nano Lett.* 8 (2008) 3498-3502.

- [16] J.S. Arellano, L.M. Molina, A. Rubio, J.A. Alonso, Density functional study of adsorption of molecular hydrogen on graphene layers, *J. Chem. Phys.* 112 (2000) 8114-8119.
- [17] S. Bhattacharya, C. Majumder, G.P. Das, Ti-decorated BC₄N sheet: A planar nanostructure for high-capacity hydrogen storage, *J. Phys. Chem. C* 113 (2009) 15783-15787.
- [18] P. Panigrahi, A. Kumar, A. Karton, R. Ahuja, T. Hussain, Remarkable improvement in hydrogen storage capacities of two-dimensional carbon nitride (g-C₃N₄) nanosheets under selected transition metal doping, *Int. J. Hydrogen Energy* 45 (2020) 3035-3045.
- [19] X. Gao, Z. Zhong, L. Huang, Y. Mao, H. Wang, J. Liu, L. Ouyang, L. Zhang, M. Han, X. Ma, M. Zhu, The role of transition metal doping in enhancing hydrogen storage capacity in porous carbon materials, *Nano Energy* 118 (2023) 109038.
- [20] T. Yildirim, S. Ciraci. Titanium-Decorated Carbon Nanotubes as a Potential High-Capacity Hydrogen Storage Medium. *Phys. Rev. Lett.* 94 (2005) 175501.
- [21] E. Durgun, S. Ciraci, W. Zhou, T. Yildirim, Transition-metal-ethylene complexes as high-capacity hydrogen-storage media, *Phys. Rev. Lett.* 97 (2006) 226102.
- [22] K. R. S. Chandrakumar, S.K. Ghosh, Alkali-metal-induced enhancement of hydrogen adsorption in C₆₀ fullerene: An ab-initio study, *Nano Lett.* 8 (2008) 13-19.
- [23] J.J. Ian, Y. Pal, P. Anas, H. Bae, H. Lee, R. Ahuja, T. Hussain, P. Panigrahi, Superalkali functionalized two-dimensional haeckelite monolayers: A novel hydrogen storage architecture, *Int. J. Hydrogen Energy* 47 (2022) 33391-33402.
- [24] P. Habibi, T. J. H. Vlugt, P. Dey, O. A. Moulto, Reversible hydrogen storage in metal-decorated honeycomb borophene oxide, *ACS Appl. Mater. Interf.* 13 (2021) 43233-43240.
- [25] C. Ataca, E. Aktürk, S. Ciraci, H. Ustunel, High-capacity hydrogen storage by metallized graphene, *Appl. Phys. Lett.* 93 (2008) 043123.
- [26] Z. Y. Liu, T. Hussain, A. Karton, S. Er, Empowering hydrogen storage properties of haeckelite monolayers via metal atom functionalization, *Appl. Surf. Sci.* 556 (2021) 149709.
- [27] E. Anikina, T. Hussain, V. Beskachko, H. Bae, H. Lee, R. Ahuja, Tuning hydrogen storage properties of carbon Ene–Yne nanosheets through selected foreign metal functionalization, *J. Phys. Chem. C* 124 (2020) 16827-16837.
- [28] E. Anikina, S.R. Naqvi, H. Bae, H. Lee, W. Luo, R. Ahuja, T. Hussain, High-capacity reversible hydrogen storage properties of metal-decorated nitrogenated holey graphenes, *Int. J. Hydrogen Energy* 47 (2022) 10654-10664.

- [29] P. Panigrahi, M. Desai, M.K. Talari, H. Bae, H. Lee, R. Ahuja, T. Hussain, Selective decoration of nitrogenated holey graphene (C_2N) with titanium clusters for enhanced hydrogen storage application, *Int. J. Hydrogen Energy* 46 (2021) 7371-7380.
- [30] Y. Wang, F. Wang, B. Xu, J. Zhang, Q. Sun, Y. Jia, Theoretical prediction of hydrogen storage on Li-decorated boron nitride atomic chains, *J. Appl. Phys.* 113 (2013) 064309.
- [31] Q.F. Li, X.G. Wan, C.G. Duan, J.L. Kuo, Theoretical prediction of hydrogen storage on Li-decorated monolayer black phosphorus, *J. Phys. D: Appl. Phys.* 47 (2014) 465302.
- [32] W. Alfalasi, Y.P. Feng, N. Tit, Enhancement of hydrogen storage using functionalized $MoSe_2$ /Graphene monolayer and bilayer systems: DFT study, *Int. J. Hydrogen Energy* 50 (2024) 1189-1203.
- [33] D.K. Sharma, S. Kumar, S. Auluck, Electronic structure, defect properties, and hydrogen storage capacity of $2H-WS_2$: A first-principles study, *Int. J. Hydrogen Energy* 43 (2018) 23126-23134.
- [34] R. Varunaa, P. Ravindran, Potential hydrogen storage materials from metal decorated 2D- C_2N : an ab-initio study, *Phys. Chem. Chem. Phys.* 21 (2019) 25311-25322.
- [35] J. Zhu, R. Yang, G. Zhang, Atomically thin transition metal dichalcogenides for the hydrogen evolution reaction, *ChemPhysMater* 1 (2022) 102-111.
- [36] X. Wang, B. Li, D.R. Bell, W. Li, R. Zhou, Hydrogen and methane storage and release by MoS_2 nanotubes for energy storage, *J. Mater. Chem. A* 5 (2017) 23020-23027.
- [37] L.G. Arellano, F.D. Santiago, A. Miranda, L.A. Perez, F. Salazar, A. Trejo, J. Nakamura, M. Cruz-Irisson, Ab initio study of hydrogen storage on metal-decorated GeC monolayers, *Int. J. Hydrogen Energy* 46 (2021) 29261-29271.
- [38] A.L. Marcos-Viquez, A. Miranda, M. Cruz-Irisson, L.A. Pérez, Tin carbide monolayers decorated with alkali metal atoms for hydrogen storage, *Int. J. Hydrogen Energy* 47 (2022) 41329-41335.
- [39] D.B. Putungan, S.-H. Lin, C.-M. Wei, J.-L. Kuo. Li adsorption, hydrogen storage and dissociation using monolayer MoS_2 : an ab initio random structure searching approach, *Phys. Chem. Chem. Phys.* 17 (2015) 11367-11374.
- [40] Q. Sun, Q. Wang, P. Jena, Y. Kawazoe, Clustering of Ti on a C_{60} Surface and Its Effect on Hydrogen Storage, *J. Am. Chem. Soc.* 127 (2005) 14582-14583.
- [41] S. Yang, M. Yoon, E. Wang, Z. Zhang, Energetics and kinetics of Ti clustering on neutral and charged C_{60} surfaces, *J. Chem. Phys.* 129 (2008) 134707.
- [42] Y. Murata, A. Calzolari, S. Heun, Tuning hydrogen adsorption on graphene by gate voltage, *J. Phys. Chem. C* 122 (2018) 11591-11597.

- [43] A. Hashmi, M.U. Farooq, I. Khan, J. Son, J. Hong, Ultra-high capacity hydrogen storage in a Li decorated two-dimensional C₂N layer, *J. Mater. Chem. A* 5 (2017) 2821-2828.
- [44] F. A. Perras, H. Thomas, P. Heintz, R. Behera, J. Yu, G. Viswanathan, D. Jing, S.S. Southern, K. Kovnir, L. Stanley, W. Huang, The structure of boron monoxide, *J. Am. Chem. Soc.* 145 (2023) 14660-14669.
- [45] E. Zintl, W. Morawietz, E. Gastinger, Bormonoxyd, *Zeitschrift für anorganische und allgemeine Chemie.* 245 (1940) 8-11.
- [46] T. Wartik, E. F. Apple, A new modification of boron monoxide, *J. Am. Chem. Soc.* 77 (1955) 6400-6401.
- [47] J. Hafner, Simulations of materials using VASP: Density-functional theory and beyond, *J. Comput. Chem.* 29 (2008) 2044-2078.
- [48] M. Ernzerhof, G. E. Scuseria, Assessment of the Perdew-Burke-Ernzerhof exchange-correlation functional, *J. Chem. Phys.* 110 (1999) 5029-5036.
- [49] S. Grimme, J. Antony, S. Ehrlich, H. Krieg, A consistent and accurate ab initio parametrization of density functional dispersion correction (DFT-D) for the 94 elements H-Pu, *J. Chem. Phys.* 132 (2010) 154104.
- [50] K. M. Rabe, J. D. Joannopoulos, Theory of the structural phase-transition of GeTe, *Phys. Rev. B.* 36 (1987) 6631-6639.
- [51] G. Henkelman, A. Arnaldsson, H. Jónsson, A fast and robust algorithm for Bader decomposition of charge density, *Comp. Mater. Sci.* 36 (2006) 354-360.
- [52] B. Mortazavi, F. Shojaei, F. Ding, X. Zhuang, Anomalous tensile strength and thermal expansion, and low thermal conductivity in wide band gap boron monoxide monolayer, *FlatChem* 42 (2023) 100575.
- [53] L. Pauling, The nature of the chemical bond. IV. The energy of single bonds and the relative electronegativity of atoms, *J. Am. Chem. Soc.* 54 (1932) 3570-3582.
- [54] T. Prohaska *et al.*, Standard atomic weights of the elements 2021 (IUPAC Technical Report), *Pure Appl. Chem.* 94 (2022) 573-600.
- [55] H. Bae, M. Park, H. Jang, Y. Kang, J. Park, H. Lee, H. Chung, C. Chung, S. Hong, Y. Kwon, B.I. Yakobson, H. Lee, High-throughput screening of metal-porphyrin-like graphenes for selective capture of carbon dioxide, *Sci. Rep.* 6 (2016) 21788.
- [56] H. Yang, H. Bae, M. Park, S. Lee, K.C. Kim, H. Lee, Fe-Porphyrin-like nanostructures for selective ammonia capture under humid conditions, *J. Phys. Chem. C.* 122 (2018) 2046-2052.

- [57] N. Kumar, H. Bae, H. Lee, T. Hussain, A. Anand, C.V. Singh, N. Tit, First-principles approach for assessing the detection of Alzheimer's biomarkers using titanium carbide MXenes, *ACS Appl. Nano Mater.* (2024) Submitted.
- [58] H. Lee, W. I. Choi, J. Ihm, Combinatorial Search for Optimal Hydrogen-Storage Nanomaterials Based on Polymers, *Phys. Rev. Lett.* 97 (2006) 056104.
- [59] A. Vaidyanathan, P. Mane, V. Wagh, B. Chakraborty, Vanadium-decorated 2D polyaramid material for high-capacity hydrogen storage: Insights from DFT simulations, *J. Energy Storage* 78 (2024) 109899.
- [60] P. Mane, S.P. Kaur, M. Singh, A. Kundu, B. Chakraborty, Superior hydrogen storage capacity of Vanadium decorated biphenylene (Bi+V): A DFT study, *Int. J. Hydrogen Energy* 48 (2023) 28076-28090.
- [61] Y.L. Liu, L. Ren, Y. He, H.P. Cheng, Titanium-decorated graphene for high-capacity hydrogen storage studied by density functional simulations, *J. Phys. Condens. Matter* 22 (2010) 445301.
- [62] V. Mahamiya, A. Shukla, N. Garg, and B. Chakraborty, High-capacity reversible hydrogen storage in scandium decorated holey graphyne: Theoretical perspectives, *Int. J. Hydrogen Energy* 47 (2022) 7870-7883.
- [63] B.J. Cid, A.N. Sosa, A. Miranda, L.A. Perez, F. Salazar, M. Cruz-Irisson, Hydrogen storage on metal decorated pristine siligene and metal decorated boron-doped siligene, *Mater. Lett.* 293 (2021) 129743.
- [64] P. Mane, S.P. Kaur, B. Chakraborty, Enhanced reversible hydrogen storage efficiency of zirconium-decorated biphenylene monolayer: A computational study, *Energy Storage* 4 (2022) e377.
- [65] P.A. Denis, F. Iribarne, Hydrogen storage in doped biphenylene based sheets, *Comput. Theor. Chem.* 1062 (2015) 30-35.
- [66] Z.Y. Liu, S. Liu, S. Er., Hydrogen storage properties of Li-decorated B₂S monolayers: A DFT study, *Int. J. Hydrogen Energy* 44 (2019) 16803-16810.
- [67] T.W. Wang and Z.Y. Tian, Yttrium-decorated C₄₈B₁₂ as hydrogen storage media: A DFT study, *Int. J. Hydrogen Energy* 45 (2020) 24895-24901.
- [68] M. Dixit, T.A. Maark, S. Pal, Ab-initio and periodic DFT investigation of hydrogen storage on light metal-decorated MOF-5, *Int. J. Hydrogen Energy* 36 (2011) 10816-10827.
- [69] A. Kundu, B. Chakraborty, Yttrium doped covalent triazine frameworks as promising reversible hydrogen storage material: DFT investigations, *Int. J. Hydrogen Energy* 47 (2022) 30567-30579.

- [70] B. Chakraborty, P. Mane, A. Vaidyanathan, Hydrogen storage in scandium decorated triazine based g-C₃N₄: Insights from DFT simulations, *Int. J. Hydrogen Energy* 47 (2022) 41878-41890.
- [71] L. Yuan, L. Kang, Y. Chen, D. Wang, J. Gong, C. Wang, M. Zhang, X. Wu, Hydrogen storage capacity on Ti-decorated porous graphene: First-principles investigation, *Appl. Surf. Sci.* 434 (2018) 843-849.
- [72] P. Mane, A. Vaidyanathan, B. Chakraborty, Graphitic carbon nitride (g-C₃N₄) decorated with Yttrium as potential hydrogen storage material: Acumen from quantum simulations, *Int. J. Hydrogen Energy* 47 (2022) 41898-41910.
- [73] S. Dong, E. Lv, J. Wang, C. Li, K. Ma, Z. Gao, W. Yang, Z. Ding, C. Wu, I.D. Gates, Construction of transition metal-decorated boron doped twin-graphene for hydrogen storage: A theoretical prediction, *Fuel* 304 (2021) 121351.
- [74] X.Y. Liang, S.P. Ng, N. Ding, C.M.L. Wu, Strain-induced switch for hydrogen storage in cobalt-decorated nitrogen-doped graphene, *Appl. Surf. Sci.* 473 (2019) 174-181.
- [75] L. Yuan, D. Wang, J. Gong, C. Zhang, L. Zhang, M. Zhang, X. Wu, L. Kang, First-principles study of V-decorated porous graphene for hydrogen storage, *Chem. Phys. Lett.* 726 (2019) 57-61.
- [76] S. Chu, L. Hu, X. Hu, M. Yang, J. Deng, Titanium-embedded graphene as high-capacity hydrogen-storage media, *Int. J. Hydrogen Energy* 36 (2011) 12324-12328.
- [77] D.Q. Lin, L.X. Wang, C.H. Song, Y.Y. Du, G.H. Chen, C. Liu, J.O. Wang, R. Wu, H.J. Qian, K. Ibrahim, H.N. Li, Potassium-doped PC₇₁BM for hydrogen storage: Photoelectron spectroscopy and first-principles studies, *Int. J. Hydrogen Energy* 46 (2021) 13061-13069.
- [78] E. Eroglu, S. Aydin, M. Simsek, Effect of boron substitution on hydrogen storage in Ca/DCV graphene: A first-principle study, *Int. J. Hydrogen Energy* 44 (2019) 27511-27528.
- [79] N. Zheng, S. Yang, H. Xu, Z. Lan, Z. Wang, H. Gu, A DFT study of the enhanced hydrogen storage performance of the Li-decorated graphene nanoribbons, *Vacuum* 171 (2020) 109011.
- [80] Q. Wu, M. Shi, X. Huang, Z. Meng, Y. Wang, Z. Yang, A first-principles study of Li and Na co-decorated T_{4,4,4}-graphyne for hydrogen storage, *Int. J. Hydrogen Energy* 46 (2021) 8104-8112.
- [81] A.N. Sosa, B.J. Cid, A. Miranda, L.A. Perez, G.H. Cocolletzi, M. Cruz-Irisson, A DFT investigation: High-capacity hydrogen storage in metal-decorated doped germanene, *J. Energy Storage* 73 (2023) 108913.
- [82] Q. Yin, G. Bi, R. Wang, Z. Zhao, K. Ma, High-capacity hydrogen storage in lithium decorated penta-BN₂: A first-principles study, *J. Power Sources* 591 (2024) 233814.

- [83] J. Hao, F. Wei, X. Zhang, L. Li, C. Chen, G. Wu, L. Wu, D. Liang, X. Ma, P. Lu, H. Song, An investigation of Li-decorated N-doped penta-graphene for hydrogen storage, *Int. J. Hydrogen Energy* 46 (2021) 25533-25542.
- [84] Q. Yin, G. Bi, R. Wang, Z. Zhao, K. Ma, High-capacity hydrogen storage in Li-decorated defective penta-BN₂: A DFT-D2 study, *Int. J. Hydrogen Energy* 48 (2023) 26288-26300.
- [85] Y. Yong, S. Hu, Z. Zhao, R. Gao, H. Cui, Z. Lv, Potential reversible and high-capacity hydrogen storage medium: Li-decorated B₃S monolayers, *Mater. Today Commun.* 29 (2021) 102938.
- [86] Y.F. Zhang, P.P. Liu, X.L. Zhu, Li decorated penta-silicene as a high capacity hydrogen storage material: A density functional theory study, *Int. J. Hydrogen Energy* 46 (2021) 4188-4200.
- [87] L. Bi, Z. Miao, Y. Ge, Z. Liu, Y. Xu, J. Yin, X. Huang, Y. Wang, Z. Yang, Density functional theory study on hydrogen storage capacity of metal-embedded penta-octa-graphene, *Int. J. Hydrogen Energy* 47 (2022) 32552-32564.
- [88] S. Haldar, S. Mukherjee, C.V. Singh, Hydrogen storage in Li, Na and Ca decorated and defective borophene: A first principles study, *RSC Adv.* 8 (2018) 20748-20757.
- [89] N. Khossossi, Y. Benhouria, S.R. Naqvi, P.K. Panda, I. Essaoudi, A. Ainane, R. Ahuja, Hydrogen storage characteristics of Li and Na decorated 2D boron phosphide, *Sustain. Energy Fuels* 4 (2020) 4538-4546.

Figure Caption

Figure 1: (a) Optimized atomic structure (top and side views) of pristine Boron-Monoxide (Pr-BO) monolayer. The dashed box represents the primitive cell as well as the simulation supercell, which belongs to a square lattice with lattice parameter $a = 7.826 \text{ \AA}$ and a basis of eight B + eight O atoms. (b) Band structure of Pr-BO showing an indirect band gap character of $E_g = 2.23 \text{ eV}$ ($X = 0.401 \text{ \AA}^{-1}$, $M = 0.803 \text{ \AA}^{-1}$, and $\Gamma = 1.371 \text{ \AA}^{-1}$). (c) Spin-polarized projected density of states of Pr-BO showing a paramagnetic semiconductor. The Fermi level has been shifted to zero and denoted by the horizontal dashed line.

Figure 2: Optimized atomic structures (top and side views) of four-metal dopants per primitive cell of BO monolayer: (a) 4Li@BO, (b) 4Na@BO, (c) 4K@BO, and (d) 4Ca@BO. The dashed box represents the primitive cell as well as the simulation supercell.

Figure 3: (a) Average binding energy per dopant atom of different metals compared to the cohesive energy and (b) Ab-initio Molecular Dynamics (AIMD) simulation plots of BO decorated with 4Li, 4Na, 4K, and 4Ca. These AIMD simulations were performed at 400 K.

Figure 4: Spin-polarized band structure and projected density of states (PDOS) of BO decorated with (a) 4Li, (b) 4Na, (c) 4K, and (d) 4Ca, where the X, M, and Γ k-vectors are 0.401, 0.803, and 1.371 \AA^{-1} , respectively. The shown electronic structures confirm the metallization of BO monolayer by metal embedding. The Fermi level has been shifted to zero and denoted by the horizontal dashed line. Bands of spin-up states (solid orange lines) and of spin-down states (dotted blue lines).

Figure 5: Charge Density Difference (CDD) showing the bond characteristics of maximally localized Wannier functions (MLWFs) of BO decorated with (a) 4Li, (b) 4Na, (c) 4K, and (d) 4Ca, where yellow and cyan isosurfaces indicate charge aggregation and depletion, respectively. Here, the isosurface level is 0.005 e/Bohr^3 .

Figure 6: Optimized atomic structures (top and side views) of the maximum hydrogen adsorption on the metal-decorated BO: (a) 16 H_2 on 4Li@BO, (b) 16 H_2 on 4Na@BO, (c) 20 H_2 on 4K@BO, and (d) 24 H_2 on 4Ca@BO.

Figure 7: (a) Average adsorption energy per H_2 molecule adsorbed on the metal-decorated BO and (b) the corresponding gravimetric density of adsorbed H_2 (wt%).

Figure 8: Thermodynamics analysis showing the average number of H_2 molecules (N_{ave}) adsorbed on (a) 4Li@BO, (b) 4Na@BO, (c) 4K@BO, and (d) 4Ca@BO as a function of applied temperature and pressure.

Table Caption

Table 1: Electronic properties of pristine and metal-functionalized BO. Δq , E_g , and M represent the Bader charge transfer, band gap, and total magnetization, respectively.

Table 2: The optimal theoretical numbers of H_2 molecules (N_T) adsorbed on the host storage materials: 4Li@BO, 4Na@BO, 4K@BO, and 4Ca@BO. These numbers are obtained from the DFT calculations and are used to compute the theoretical storage (C_T) capacities. Meanwhile, N_a and N_d represent the amount of adsorbed H_2 molecules under the adsorption ($P = 30 \text{ atm}$ and $T = 25 \text{ }^\circ\text{C}$) and desorption (3 atm and $T =$

100 °C) conditions, respectively (equations 4-6). The practical number of H₂ molecules (N_p) that can be reversibly stored/released is given by N_a-N_d. The effective storage capacity (C_E) is then computed based on N_p using equation (3).

Table 3: Comparison between different hydrogen storage systems in terms of theoretical number of adsorbed H₂ molecules per simulation cell (N_T), average adsorption energy per H₂ molecule (E_{ads}), and theoretical H₂ gravimetric capacity (C_T).

Table 1

System	Δq (e/MI)	E _g (eV)	M (μ _B)
Pristine BO	NA	2.183 (↑)(↓)	0.00
BO:4Li	0.695	Metallic	1.062
BO:4Na	0.479	0.000 (↑) 0.182 (↓)	0.030
BO:4K	0.462	0.000 (↑) 0.230 (↓)	2.109
BO:4Ca	0.856	Metallic	0.00

Table 2

Storage material	C _T (wt%)	N _T (molecule)	N _a (molecule)	N _d (molecule)	N _p (molecule)	C _E (wt%)
4Li@BO	11.75	16	15.53	2.07	13.46	9.88
4Na@BO	9.52	16	6.77	0.13	6.65	3.96
4K@BO	9.80	20	18.16	1.10	17.06	8.53
4Ca@BO	11.43	24	23.37	3.68	19.75	9.78

Table 3

Hydrogen Storage System	n	E_{ads} (eV)	C_T (wt%)
Li-decorated BO (this work)	16	-0.205	11.75
Na-decorated BO (this work)	16	-0.175	9.52
K-decorated BO (this work)	20	-0.185	9.80
Ca-decorated BO (this work)	24	-0.204	11.43
V-decorated 2DPA-I [59]	7	-0.44	7.29
V-decorated biphenylene [60]	7	-0.47	10.30
Ti-decorated graphene [61]	8	-0.42	7.80
Li-decorated B@r ₅₇ haeckelite [26]	12	-0.16	10.00
Sc-doped Holey graphyne [62]	5	-0.36	9.80
Li-decorated B-doped siligene [63]	4	-0.17	12.71
Ti-decorated C ₂ N [29]	10	-0.28	6.80
Zr-decorated biphenylene [64]	9	-0.40	9.95
Li-decorated biphenylene [65]	12	-0.20	7.40
Li-decorated B ₂ S honeycomb [66]	12	-0.14	9.10
Y-decorated C ₄₈ B ₁₂ [67]	72	-0.46	7.51
Li-decorated MOF-5 [68]	18	–	4.30
Y-decorated covalent triazine frameworks [69]	7	-0.33	7.30
Sc-decorated g-C ₃ N ₄ [70]	7	-0.39	8.55
Ti-decorated graphene [71]	8	-0.46	6.11
Y-decorated g-C ₃ N ₄ [72]	9	-0.33	8.55
Ti-decorated B-doped twin-graphene [73]	8	-0.20	4.95
Co-decorated N-doped graphene [74]	28	-0.19	11.36
V-decorated porous graphene [75]	6	-0.56	4.58
Ti-decorated graphene [76]	8	-0.21	6.30
K-doped PC ₇₁ BM [77]	45	-0.14	6.22
Ca-decorated DCV graphene [78]	14	-0.10	5.80
Li-decorated graphene nanoribbons [79]	8	-0.24	3.80
Li-decorated T _{4,4,4} -graphyne [80]	16	-0.20	10.46
K-decorated Ga-doped germanene [81]	36	-0.19	8.19
Li-decorated P-BN ₂ [82]	28	-0.16	13.27
Li-decorated N-doped penta-graphene [83]	12	-0.24	7.88
Li-decorated defective penta-BN ₂ [84]	16	-0.14	9.17
Li-decorated B ₃ S [85]	12	-0.17	7.70
Li-decorated penta-silicene [86]	12	-0.22	6.42
Li-decorated penta-octa-graphene [87]	3	-0.22	9.90
K-decorated SnC [38]	6	-0.20	5.50
Li-decorated borophene [88]	10	-0.36	9.00

Li-decorated boron phosphide [89]	16	-0.19	7.40
Li-decorated defected biphenylene [7]	14	-0.20	8.75

Figures

Light-Metal Functionalized Boron Monoxide Monolayers as Efficient Hydrogen Storage Material: Insights from DFT Simulations

Wael Othman^{1,2}, Wadha Al Falasi^{3,4}, Tanveer Hussain⁵, and Nacir Tit^{3,4*}

¹Engineering Division, New York University Abu Dhabi, Abu Dhabi, United Arab Emirates

²Mechanical and Aerospace Engineering, Tandon School of Engineering, New York University, NY 10012, USA

³Physics Department, UAE University, Al Ain, United Arab Emirates

⁴Water Research Center, UAE University, Al-Ain, United Arab Emirates

⁵School of Science and Technology, University of New England, Armidale, New South Wales, 2351, Australia

*Corresponding Author: ntit@uaeu.ac.ae

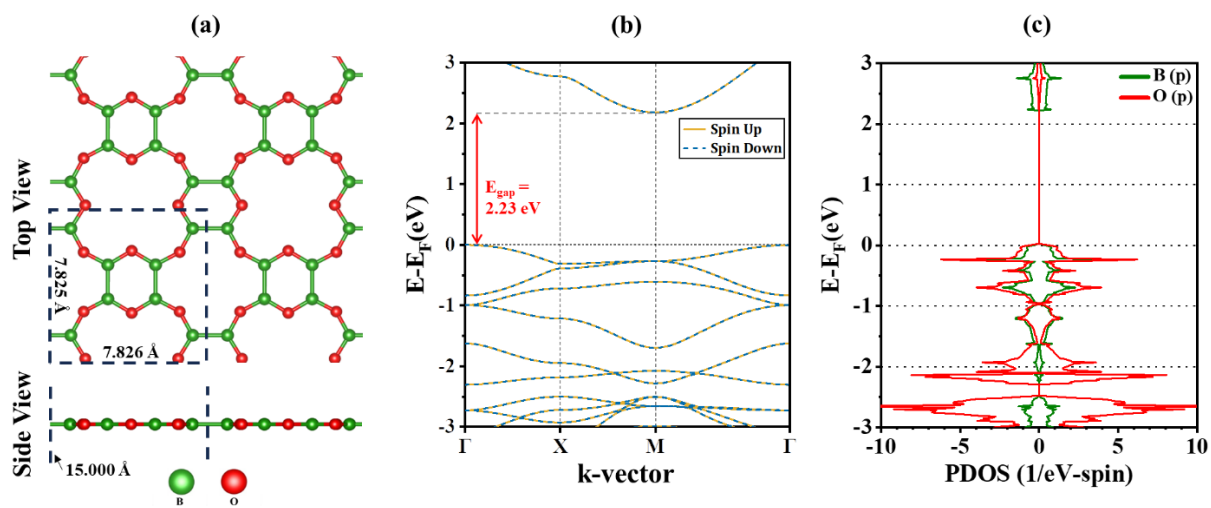


Figure 1

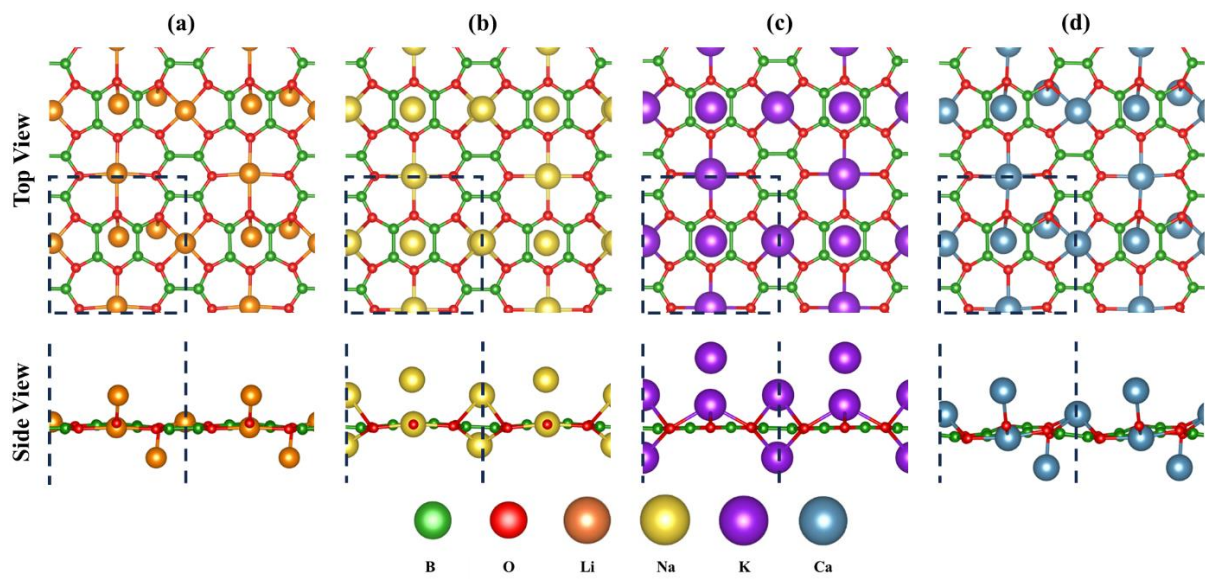


Figure 2

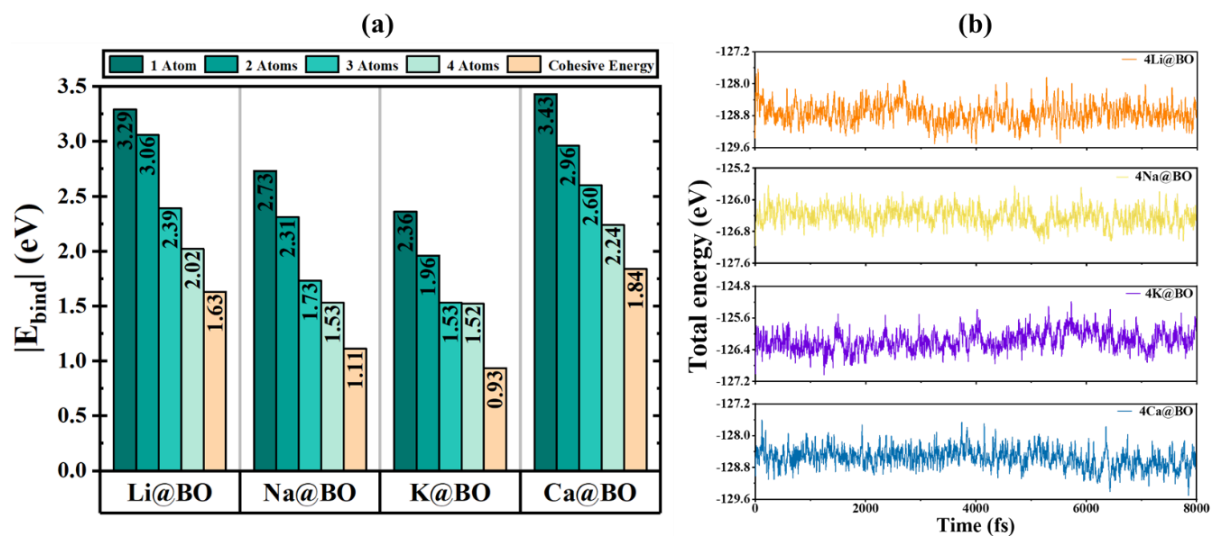


Figure 3

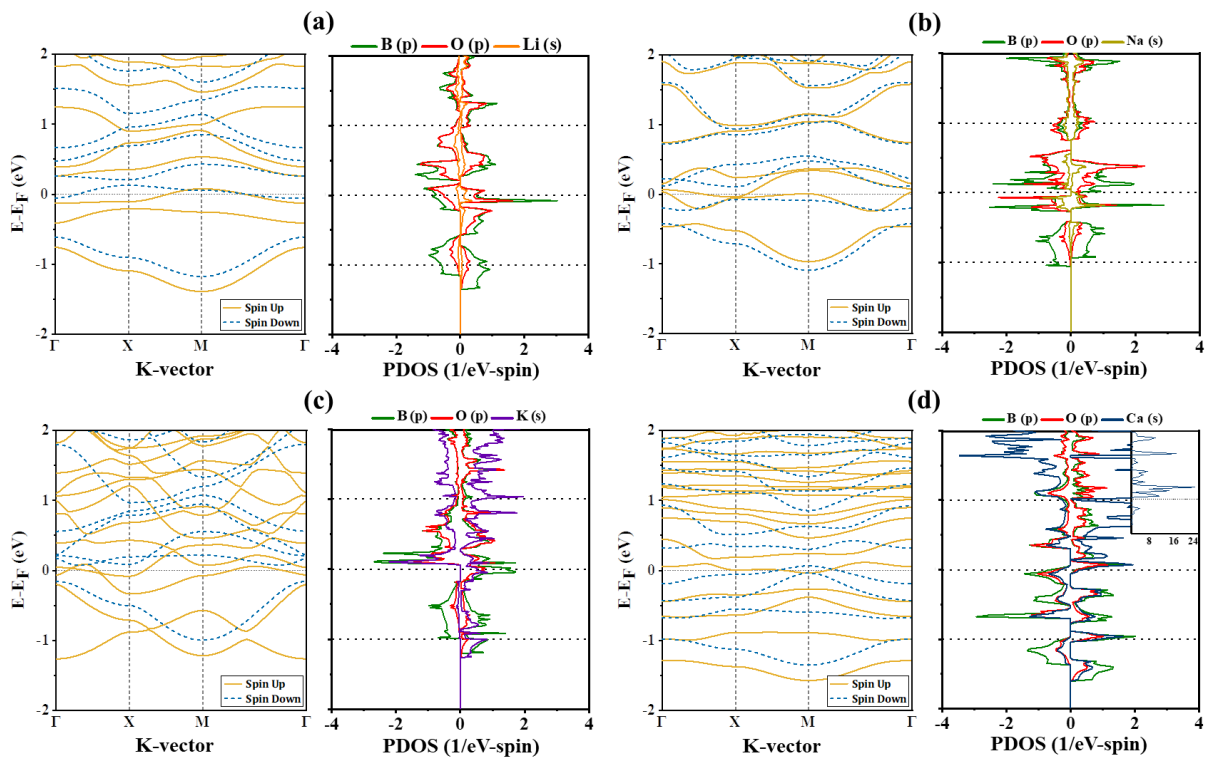


Figure 4

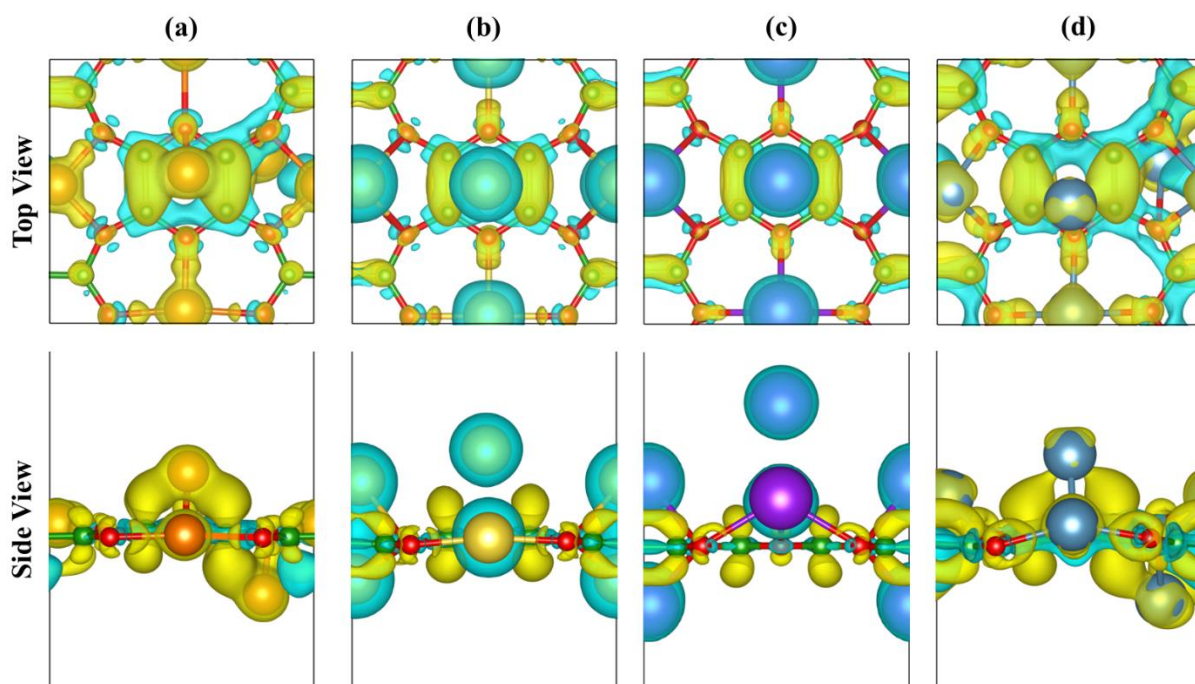


Figure 5

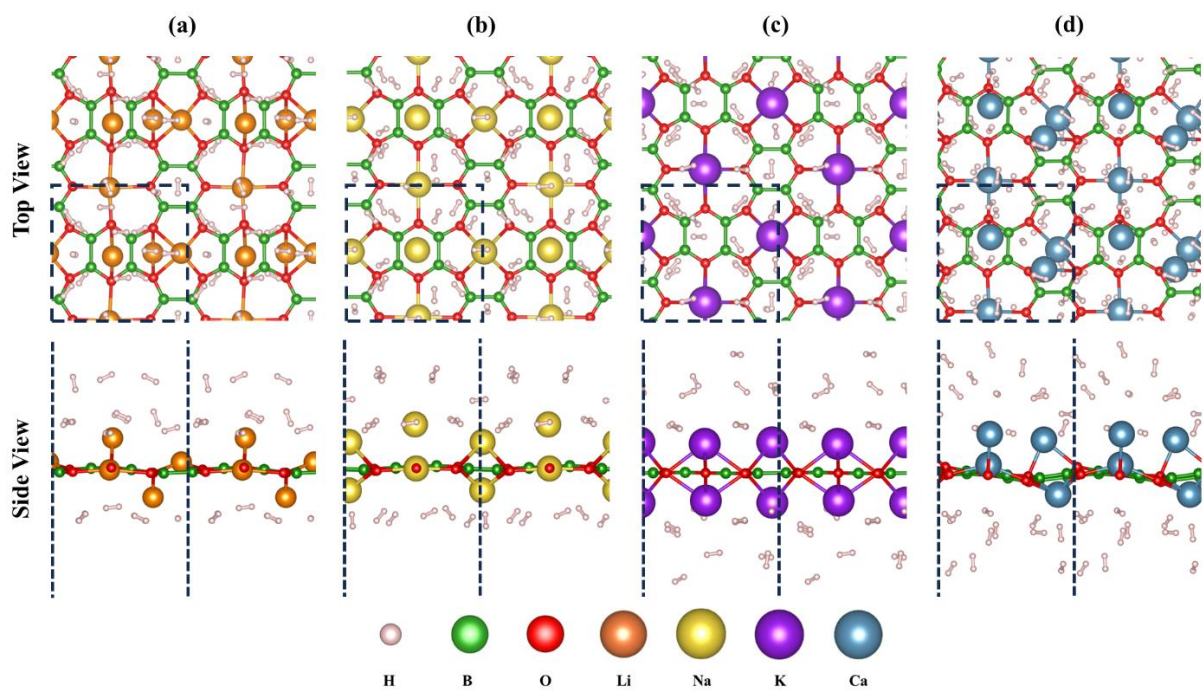


Figure 6

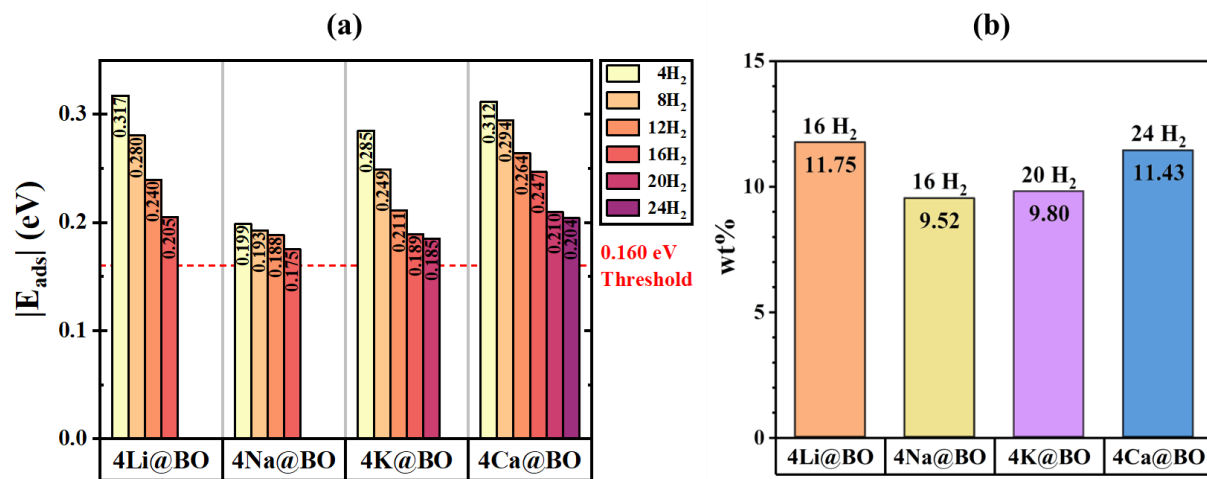


Figure 7

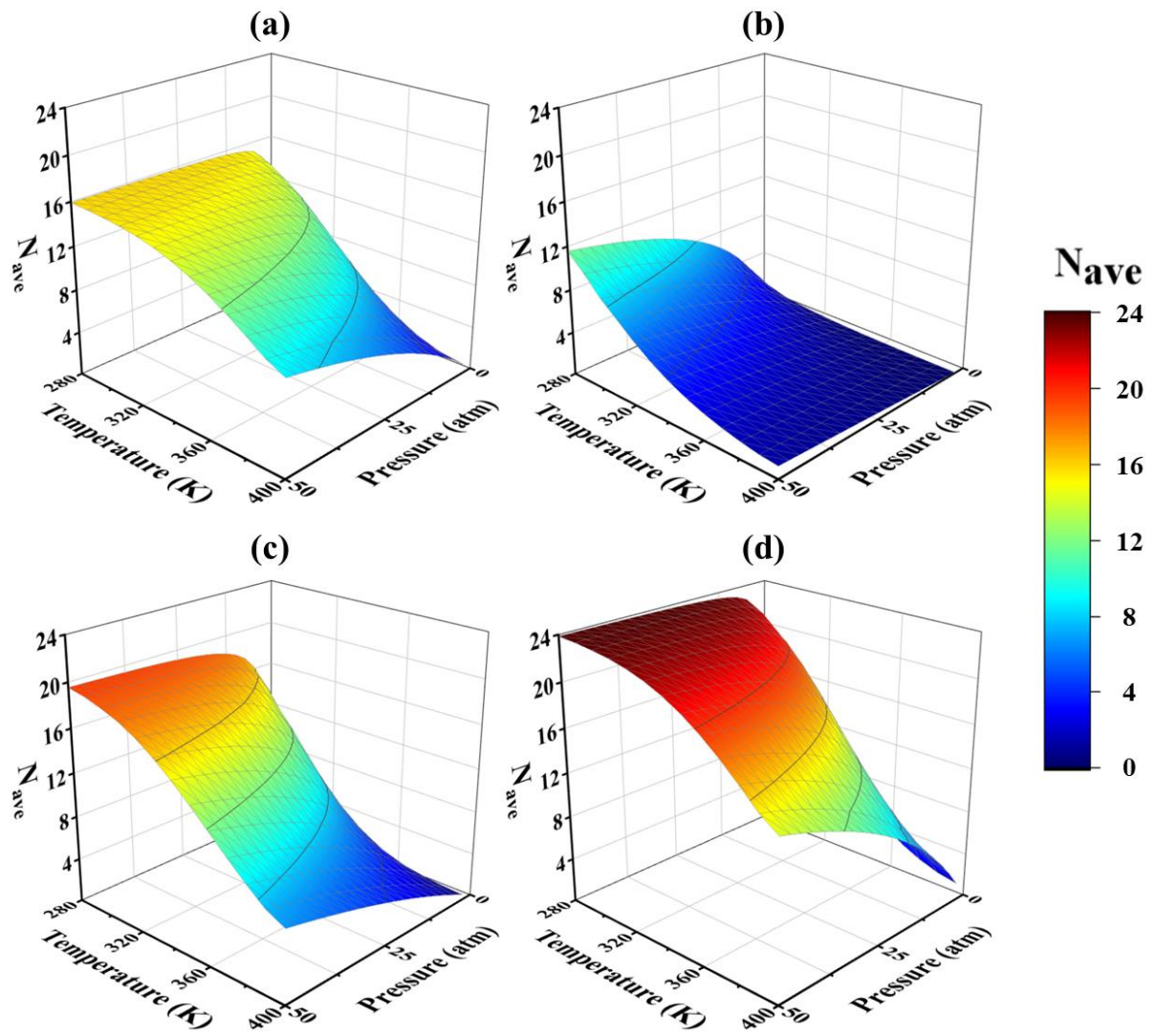


Figure 8